

## Supplementary Information

### **Twin-driven thermoelectric figure-of-merit enhancement of Bi<sub>2</sub>Te<sub>3</sub> Nanowires**

Ho Sun Shin<sup>a</sup>, Seong Gi Jeon<sup>b</sup>, Jin Yu<sup>b</sup>, Yong-Sung Kim<sup>a,c</sup>, Hyun Min Park<sup>a,c</sup> and Jae Yong Song<sup>a,c\*</sup>

<sup>a</sup> Center for Nanomaterials Characterization, Korea Research Institute of Standards and Science, Daejeon, 305-340, Republic of Korea.

<sup>b</sup> Department of Materials Science and Engineering, Korea Advanced Institute of Science and Technology, Daejeon 305-701 Republic of Korea.

<sup>c</sup> University of Science and Technology, Daejeon 305-350, Republic of Korea.

\*Corresponding Author: jysong@kriss.re.kr (J.Y.S.)

#### ***1. Fabrication of the MTMP structure***

The membrane-type MTMP was fabricated on low-stress silicon nitride (500 nm thick) deposited on silicon wafer using a lithography method. Nano-patterns, which consisted of a symmetric pair of Pt nanoheaters, current carrying electrodes, and Pt thermometers, were formed by a UV stepper. The Pt thermometers close to the center were also used as the voltage measurement probes (termed inner electrodes) for the four probe electrical conductivity measurements. The Pt line width was defined to be 0.5 μm for the thermometers and the

nanoheaters, respectively. The thickness of the Pt line was 40 nm and 10 nm-thick Ti was used as an adhesive layer between Pt and silicon nitride. The back-side silicon beneath the nanopattern was etched away by an anisotropic wet etching process in a KOH solution. The membrane structure can enhance the measurement sensitivity of temperature.

To realize the suspended bridge-type MTMP, we coated a thick PR layer as a protecting mask on the membrane-type MTMP and performed reactive ion etching process to remove the unnecessary area of silicon nitride around the nanopattern.

We used a micro-manipulation system to locate a NW onto the targeted position of MTMP in air environment [Figure S9]. We steered a tungsten tip where a NW was attached by Van der Waals forces. This allowed us to pick and place a BT NW into the targeted position without any contamination or damage. After locating a NW on the MTMP, we make electrical contacts, as follows; first, after spin-coating of polymethylmethacrylate (PMMA, 950 k, 4%), the substrates were softly baked at 443 K for 2 min. E-beam lithography was performed to define the electrical contact pattern on the NW and then the development process was carried out in MIBK:ethanol = 1:1 solution. Then Ni and Al layers (100-nm Al and 10-nm Ni) were sequentially deposited by a RF-sputtering system. Then a lift-off process was conducted in acetone. The ohmic contact between the NW and the Pt electrodes was formed using Ni/Al metallization, as shown in the typical I-V characteristic of TF NW at 2 K and 300 K [Figure S10]

## ***2. Temperature calibration***

The electrical resistances of two Pt thermometers were measured by varying the environmental temperature in the range of 40 to 300 K, as shown in Fig.S11, and the temperature coefficients of

resistance (TCRs) of the Pt thermometers were determined by linear fitting of the resistance to temperature relation. The TCR values were measured for all the MTMPs with slightly different Pt resistance. For example, the TCR of a thermometer was measured to be  $0.1429 \pm 0.0011 \text{ } \Omega/\text{K}$  from a linear fitting with the coefficient of determination of 0.999, as shown in Figure S11.

### ***3. Measurement of TE properties***

The temperature gradient between two thermometers was generated using a DC current source (Keithley, 6220) connected to one of the nanoheaters shown in Fig.1(a). The corresponding TE voltage was recorded by a nanovoltmeter (Keithley, 2182A) and two lock-in amplifiers (Signal recovery, 5210) simultaneously read the resistance values of both thermometers (inner electrodes). A switching module (scanner relay) made it possible for the inner electrodes to play the dual roles of a thermometer and a voltage probe without signal interference: the two lock-in units read the temperature difference in the relay-on state of the scanner relay while the nanovoltmeter measured the TE voltage between the inner electrodes in the relay-off state of the scanner relay. One lock-in unit was operated at 32.7 Hz and the other one at 42.7 Hz. As shown in Figure S12, Seebeck voltage measurement was repeated for the two nanoheaters under a given temperature gradient. The Seebeck voltages measured from the two different nanoheaters showed the same values but opposite sign.

The electrical conductivity of a single NW was measured on the membrane-type MTMP using a four-point probe method. The outer electrodes were used as DC current source and drain while the voltage drop was measured between the inner electrodes by the nanovoltmeter.

For the sake of measuring the thermal conductivity of NWs in a steady state heat flow, we used a one-dimensional conduction model,  $Q = G\Delta T$ , where  $Q$ ,  $\Delta T$ , and  $G$  are the heat dissipation (W, J/s) transferring through the NW, temperature difference (K) between hot and cold junctions, and thermal conductance (W/K) of the NW. Here, the heat dissipations of heat radiation and convective residual gas are assumed to be negligible because the temperature in the range of 40 to 300 K was not so high and the vacuum was less than  $1 \times 10^{-5}$  torr.

For the MTMP without NWs, the heat dissipation ( $Q_1$ ) in the steady state can be written as follows,

$$Q_1 = G_1(T_{h,1} - T_o) \quad (\text{Eq.1})$$

Here,  $Q_1$  is the heat dissipation at the hot junction,  $G_1$  is temperature-dependent thermal conductance through the silicon nitride beams connected to the heat source,  $T_{h,1}$  and  $T_o$  are the temperatures of hot junction and environment (heat-sink), respectively.

In a similar vein, for the MTMP with the NW connected between hot and cold junctions shown in Fig.1(b), the heat dissipation ( $Q_2$ ) can be described, as follows,

$$Q_2 = G_1(T_{h,2} - T_o) + G_{NW}(T_{h,2} - T_{c,2}) \quad (\text{Eq.2})$$

Here,  $G_{NW}$  is the temperature-dependent thermal conductance of the NW,  $T_{h,2}$  and  $T_{c,2}$  are the temperatures at the hot and cold junctions where the NWs are interconnected.

Using (Eq.2), the thermal conductance of NWs can be calculated, as follows,

$$G_{NW} = \frac{Q_2 - G_1(T_{h,2} - T_o)}{(T_{h,2} - T_{c,2})} \quad (\text{Eq.3})$$

The power dissipations ( $Q_1$  and  $Q_2$ ) at the hot junction are directly measured by using the four point probe electrodes on the nanoheater shown in Fig. 1(f). For the NWs-carrying MTMP, we measure  $Q_2$ ,  $T_{h,2}$ , and  $T_{c,2}$ , at temperature ( $T_0$ ). And the  $G_1$  can be evaluated by (Eq.1) after the NWs are cut using an atomic force microscope (AFM) tip. It is reasonably assumed that the thermal conductance ( $G_1$ ) remains constant within the temperature range of 5 K. Using the AFM tip, the NW was readily cut without any damage on the MTMP. Figure S13 shows the SEM images of the BT NWs before and after the AFM cutting.

Finally, the thermal conductivity of the NW ( $k_{NW}$ ) is derived using the geometry of the NW as follows,

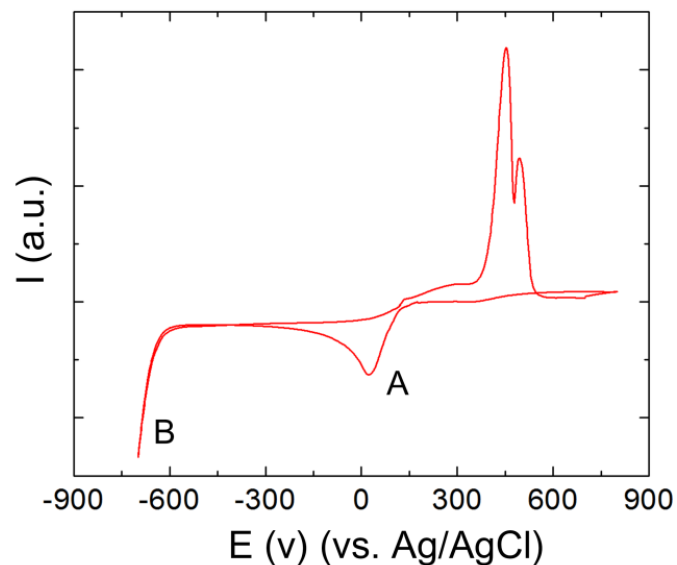
$$k_{NW} = G_{NW}(T_0)(L/A) \quad \text{Eq.(4a)}$$

$$k_{NW} = G_{NW}(T_0)(L_n/\Sigma A_n) \quad \text{Eq.(4b)}$$

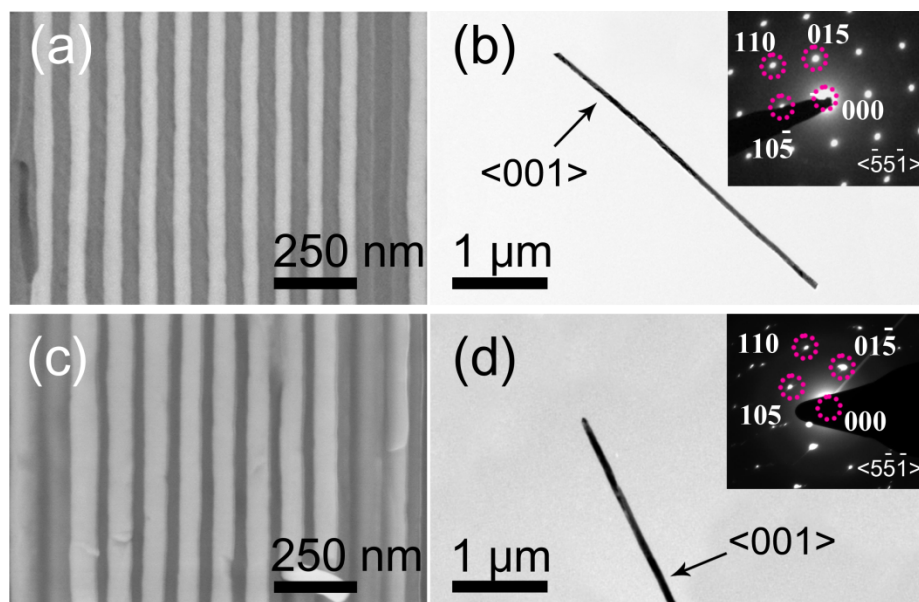
Here,  $k_{NW}$  is the thermal conductivity of a NW,  $A$  is the cross-sectional area of a NW, and  $L$  is the length of a NW. When we use a NW bundle (composed of several NWs), the thermal conductivity of a single NW can be written as Eq.(4b). Here,  $n$  is the number of NWs.

Figure S14 shows the example of thermal conductivity measurement. Figure S14(a) shows the variations of electrical resistance of two Pt thermometers with stepwise heating time. Each heating step includes 120 data points; however, we only used the last 40 points to determine the averaged resistance for each step because the MTMP needs time to reach a steady state of heat transfer. Figure S14(b) shows the variation of temperature change ( $\Delta T$ ) between two thermometers with heater power ( $Q$ ) for TF NWs. The thermal conductance was determined by the slope of  $Q = G\Delta T$ . Figure S14(c) shows the variations of thermal conductances for the MTMP and the MTMP including NWs. The thermal conductance of the NWs was determined by

subtracting the thermal conductance ( $G_1$ , slope of blue squared data) of the MTMP without the NWs from that ( $G_2$ , slope of red circled data) of the MTMP including the NWs (dashed line), according to Eq.(3). Finally, the thermal conductivity of a NW was calculated by Eq.(4b).



**Figure S1.** (a) A cyclic voltammogram for BT NW. The peak A at  $V_R$  of +0.017 indicates the formation of  $\text{Bi}_2\text{Te}_3$ , and the peak B hydrogen evolution.



**Figure S2.** SEM images of (a) TF NWs and (c) TC NW electrodeposited within AAM at  $V_R=+0.017$  V and  $V_R=+0.120$  V, respectively. Bright-field TEM images of (b) TF NW and (d) TC NW. The insets in (b) and (d) indicate the corresponding SAED patterns. The SAED pattern was obtained using a 10  $\mu\text{m}$ -aperture.

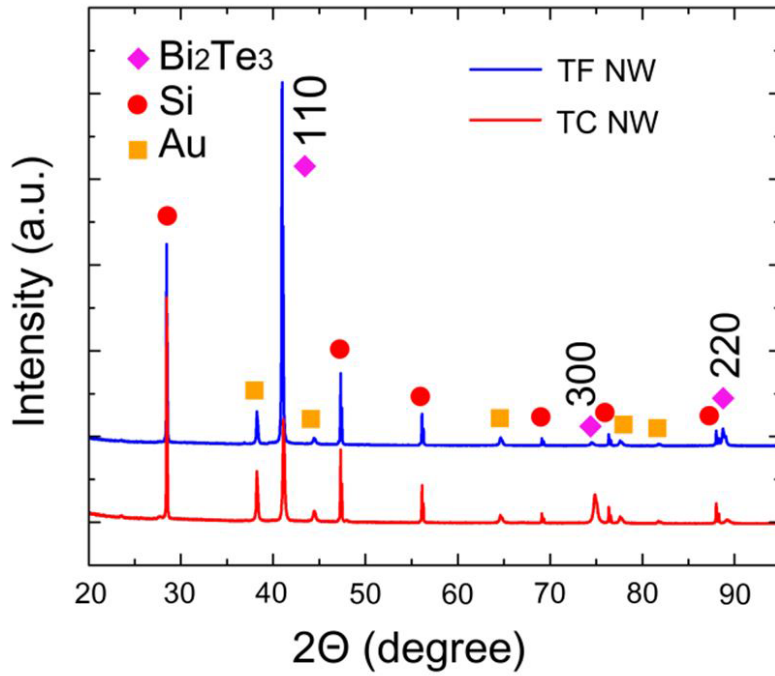


**Figure S3.** XRD patterns of TF and TC  $\text{Bi}_2\text{Te}_3$  NWs within the AAM.

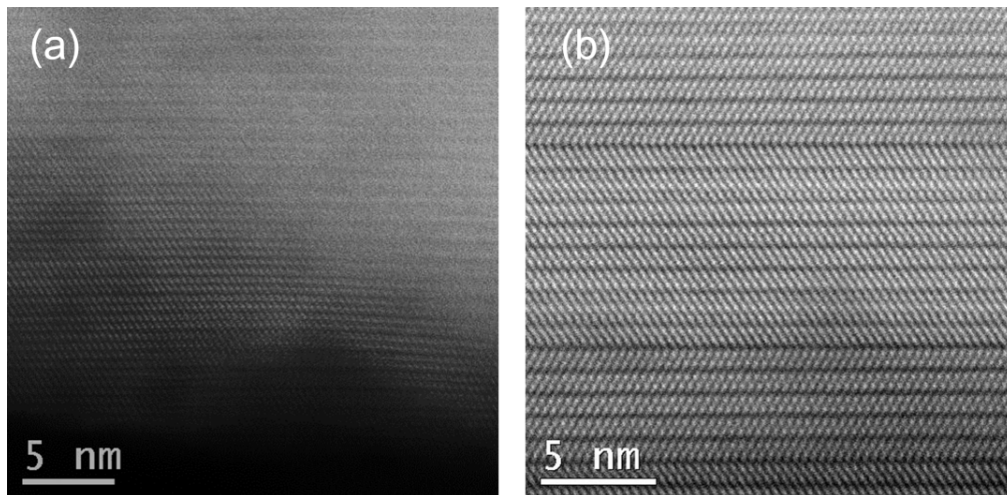


**Figure S4.** HAADF-STEM images of (a) TFHT and (b) TCHT after a heat treatment at 673 K for 2 hours.

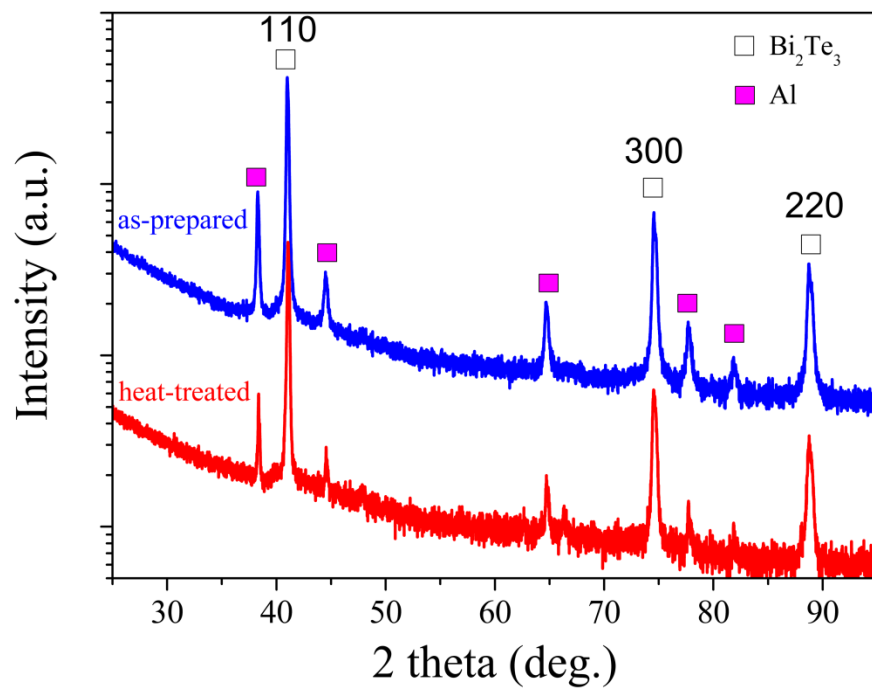


**Figure S5.** XRD patterns of TF NWs before and after a heat treatment at 673 K for 2 hours in vacuum.

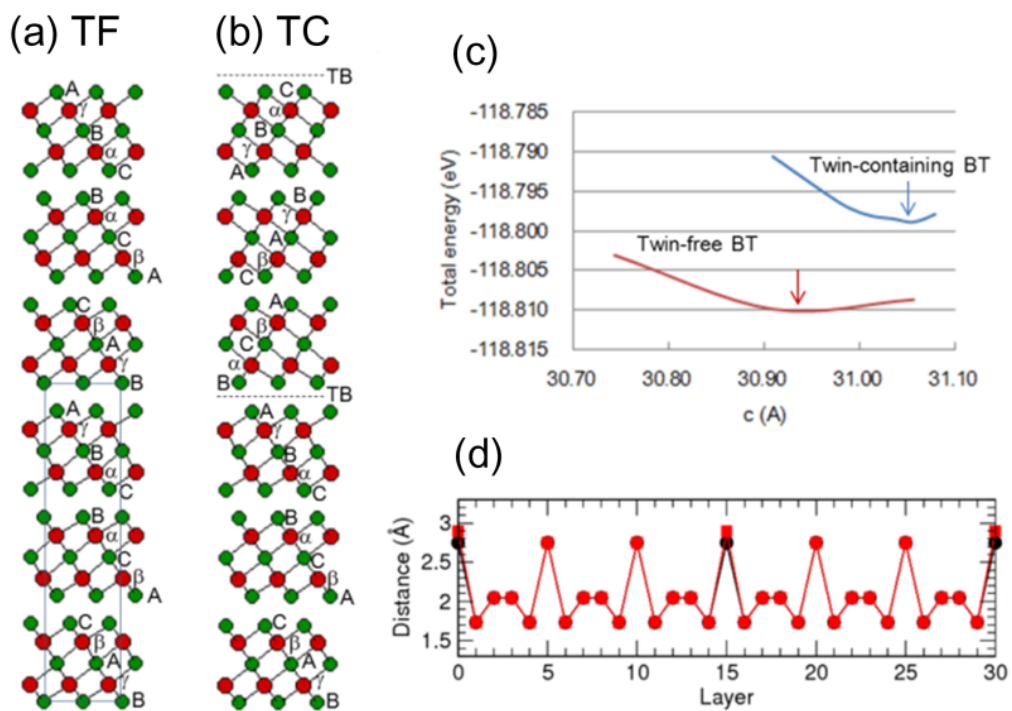


**Figure S6.** Schematic diagrams of atomic structures of (a) TF and (b) TC BT supercells. The rectangle in (a) and the dashed lines in (b) indicate the unit cell of three quintuple-layers and the twin, respectively. (c) Calculated total energies of the twin-containing BT with respect to the unit cell length ( $c$ ). (d) Calculated interlayer distances of the TF (squares) and TC (circles) BT.

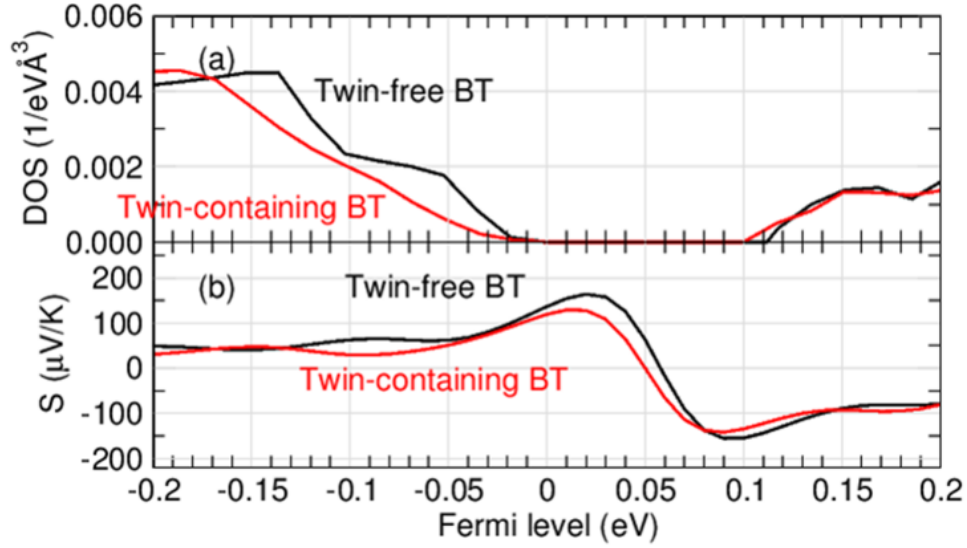


**Figure S7.** Calculated (a) electronic density-of-states (DOS) and (b) Seebeck coefficients of the TF (black line) and TC (red line) BT, as a function of the Fermi level.

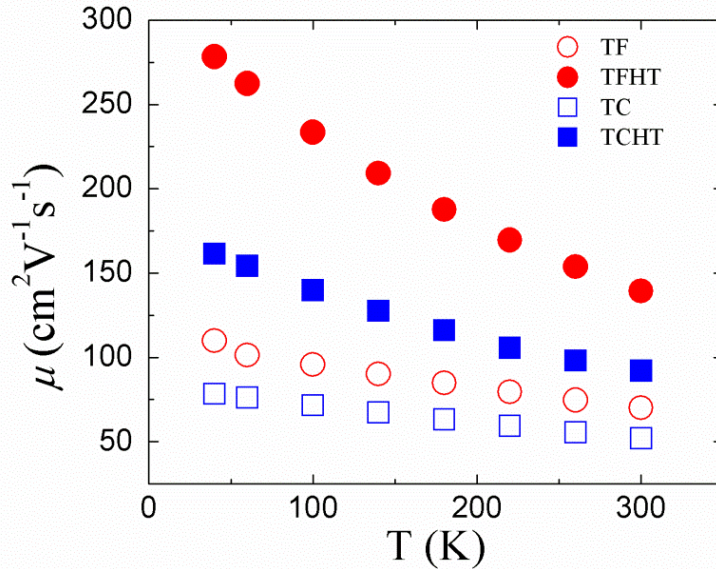


**Figure S8.** Variations of carrier mobility ( $\mu$ ) of TF, TC, TFHT, and TCHT NWs with temperature.

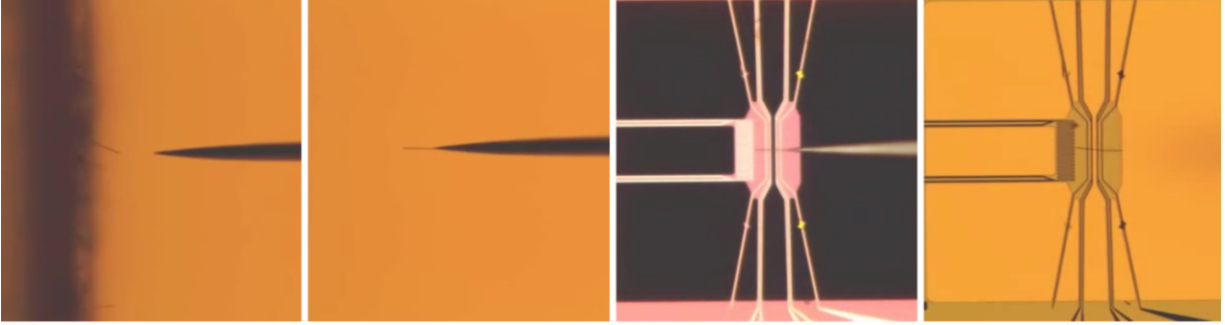


**Figure S9.** Optical images of (a) tungsten tip approaching the nanowire, (b) a nanowire attached on the tungsten tip, (c) tungsten tip placing the nanowire onto the MTMP, and (d) nanowire positioned on the center of the MTMP.

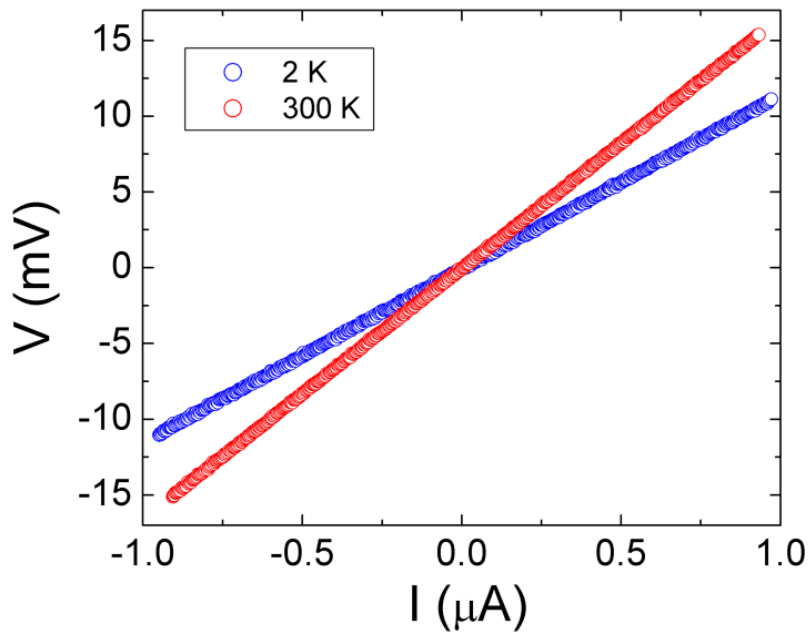


**Figure S10.** I-V curves of TF NW at 2 and 300 K.

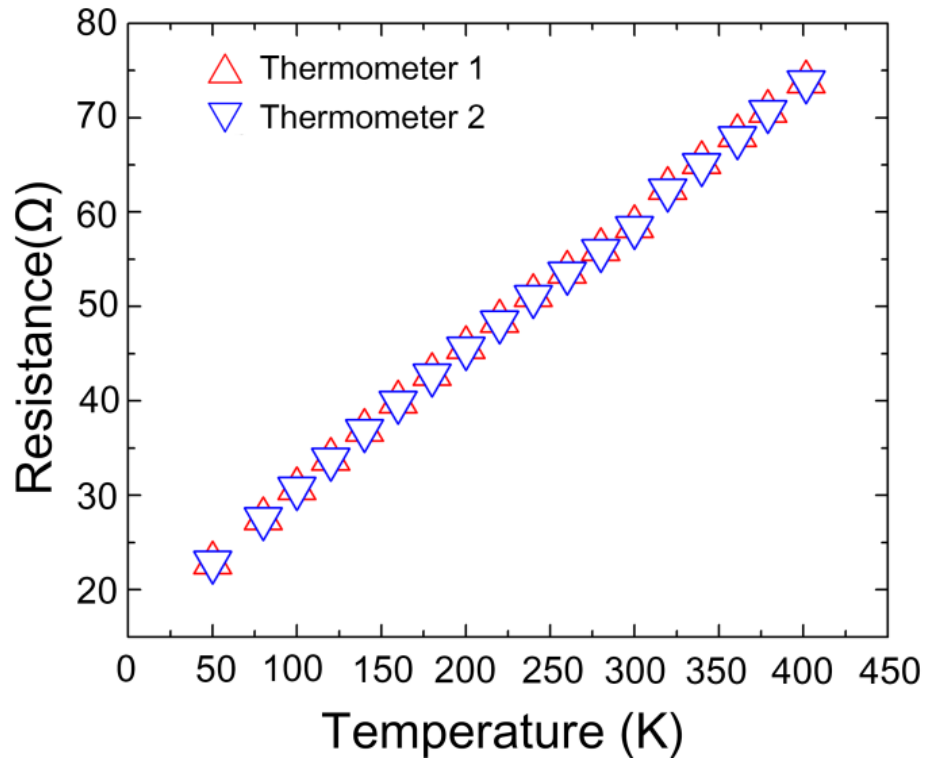


**Figure S11.** Variations of electrical resistances of Pt thermometers at hot and cold junctions with temperature. The slope determines the TCRs of Pt thermometers.

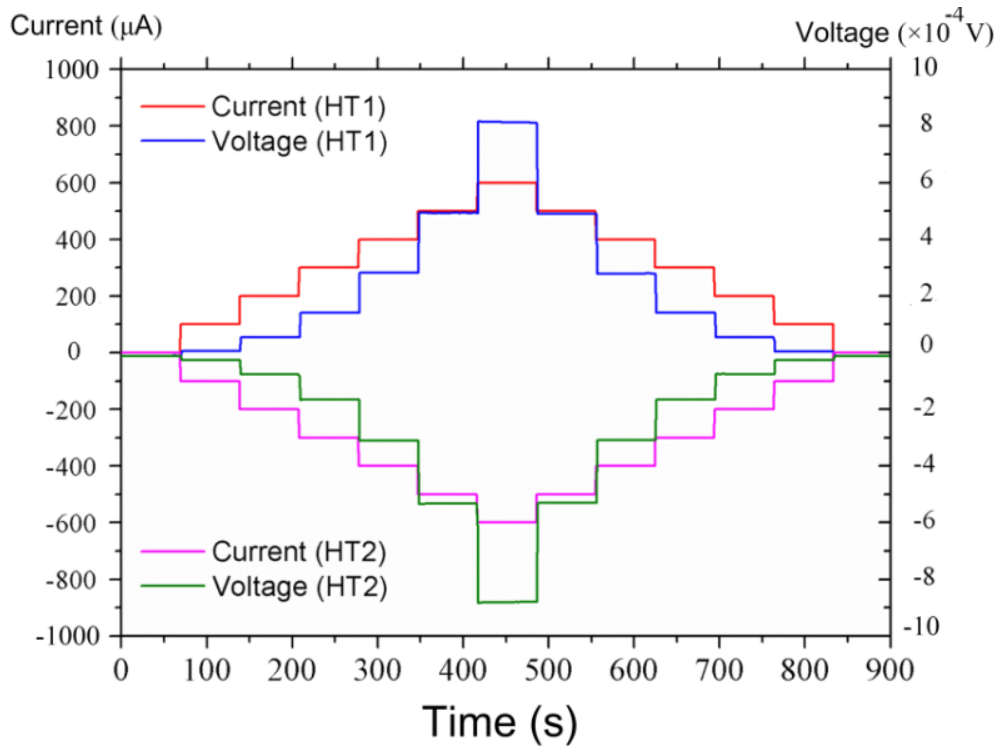


**Figure S12.** Variations of thermoelectric voltages with stepwise changing current of heaters (HT1 and HT2). When the heat flow is reversed by alternative heating (HT1 or HT2), the polarity of thermoelectric voltages is reversed with the same magnitude.

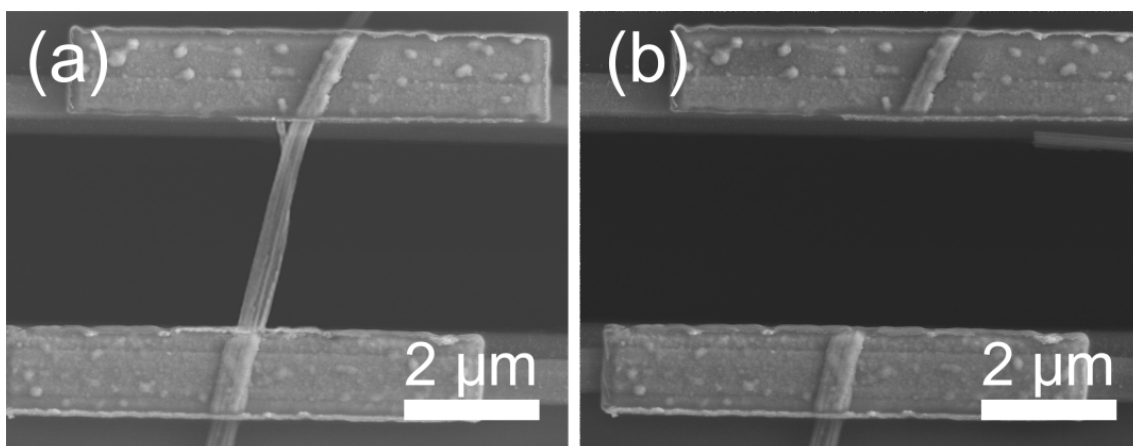


**Figure S13.** SEM images of a BT NW bundle with metal contacts between hot and cold junctions (a) before and (b) after AFM cutting.

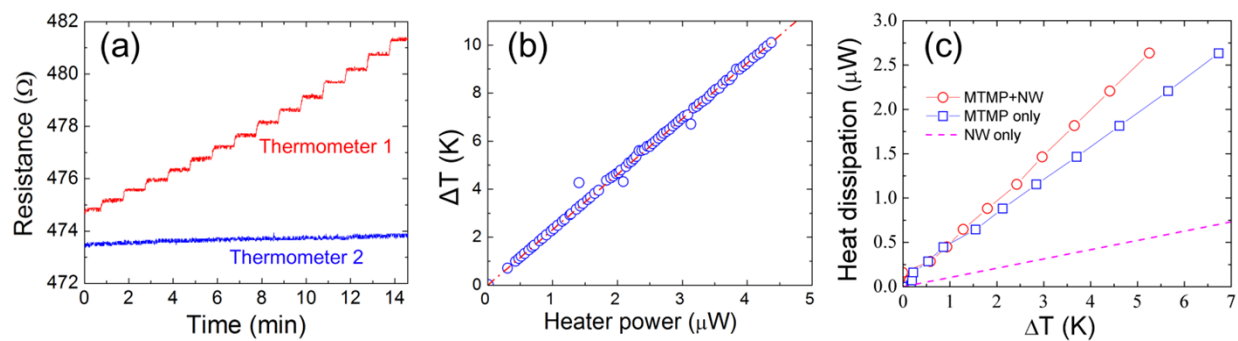


**Figure S14.** Variations of (a) electrical resistance of two Pt thermometers with the heater current of MTMP without a NW, (b) temperature difference ( $\Delta T$ ) between hot and cold junctions with the heater power, and (c) heat dissipations with temperature difference by NW, MTMP, and MTMP containing NWs, respectively.